Journal of Industrial and Engineering Chemistry 45 (2017) 5–10

Contents lists available at ScienceDirect

Journal of Industrial and Engineering Chemistry

journal homepage: www.elsevier.com/locate/jiec

Short communication

Intracellular delivery of recombinant proteins via gold nanoparticle–DNA aptamer composites is independent of the protein physicochemical properties and cell type

Ji-Hyun Yeom[a,1], Minju Joo[a,1], Boeun Lee[a], Keun P. Kim[a], Nam-Chul Ha[b], Yoonkyung Park[c], Jeehyeon Bae[d,*], Kangseok Lee[a,*]

[a] Department of Life Science, Chung-Ang University, Seoul 06974, Republic of Korea
[b] Department of Agricultural Biotechnology, Seoul National University, Seoul 08826, Republic of Korea
[c] Department of Biomedical Science, Chosun University, Gwangju 61452, Republic of Korea
[d] School of Pharmacy, Chung-Ang University, Seoul 06974, Republic of Korea

ARTICLE INFO

Article history:
Received 7 July 2016
Received in revised form 26 September 2016
Accepted 28 September 2016
Available online 8 October 2016

Keywords:
DNA aptamer
Gold nanoparticle
Protein delivery
Intravenous delivery

ABSTRACT

Here, we report that the gold nanoparticle–DNA aptamer (AuNP–Apt) conjugate-based system can efficiently deliver recombinant proteins into mammalian cells in a manner independent of their size, isoelectric point, and cellular localization. Additionally, AuNP–Apt system-assisted protein delivery can be effective on primary and stem cells, indicating that its use is not limited to fast-dividing cells. We further show that the intravenously administered AuNP–Apt system can deliver proteins into rat organs. Our findings show that this system can serve as a simple, efficient, and versatile platform for the delivery of recombinant proteins into mammalian living systems.

Introduction

Compared with small-molecular drugs, protein therapy has several advantages, including higher specificity, greater activity, and less toxicity [1,2]. However, the use of many therapeutic proteins has been limited by their poor membrane permeability, susceptibility to endosomal internalization, instability, and immunogenicity [1,3–5]. One strategy for overcoming the poor membrane permeability of target proteins is to synthetically attach genetically fused proteins with cell-penetrating peptides, such as TAT-derived peptides, arginine-rich peptides, and amphiphilic peptides, to improve intracellular protein delivery [6]. Despite the improvement in their membrane permeability, however, these protein drugs linked to cell-permeable sequences have raised a problem in their clinical development because their unique cell-permeable properties can cause toxicity, especially with chronic use [7]. To achieve high therapeutic performance, several delivery vehicles for proteins have been developed based on different nanomaterials, such as polymeric, lipid-based, and inorganic nanoparticles (for a recent review, see Ref. [2]). However, these systems require a complex process of linking the target protein to a nanocarrier, which may alter the structure and function of the protein [8–11]. Furthermore, not only do most of these nanocarrier-based systems cause cytotoxicity in vivo but they can be used only for the delivery of a subset of proteins with certain properties [1,4,5]. It has also been suggested that these nanocarriers are effective on rapidly growing mammalian cells, the membrane of which is more susceptible to penetration by nanocarriers [12].

For these reasons, we previously developed a protein delivery system based on gold nanoparticles (AuNPs) functionalized with a DNA aptamer (AuNP–Apt) [13], by combining the properties of aptamers (e.g., high binding affinity, low immunogenicity, and long-term stability) [14] with the unusually efficient cellular uptake that results from conjugating AuNPs with a DNA oligonucleotide [15,16]. These properties of AuNP and RNA aptamer also have been utilized for the development of targeted delivery of a drug [17]. In this study, we investigated the delivery efficiency of this system in relation to the intrinsic properties of the

* Corresponding authors.
E-mail addresses: jeehyeon@cau.ac.kr (J. Bae), kangseok@cau.ac.kr (K. Lee).
[1] These authors contributed equally to this work.

http://dx.doi.org/10.1016/j.jiec.2016.09.043
1226-086X/

delivered proteins, such as their size, isoelectric point (pI), and cellular localization. We also tested the ability of this system to deliver proteins into mammalian primary and stem cells that are known to be difficult to transfect with biomaterials, as well as into organs of rat.

Materials and methods

Synthesis of AuNP–Apt conjugates and preparation of AuNP–Apt–protein complexes

The Histidine aptamer-conjugated AuNP (AuNP–Apt^{His}) and AuNP–Apt^{His}–protein complex were prepared according to previously described procedures [13]. The procedure for preparation of recombinant proteins has been previously described and is shown in Table 1. C-terminally hexahistidine-tagged HPA3P peptide was synthesized and purified as described previously [18]. The size and ζ potential of nanoparticles were measured as described previously [13].

Visualization of protein uptake by AuNP–Apt conjugates

Visualization of recombinant proteins in cultured cells was carried out as previously described [13]. In brief, to detect the delivery of the proteins into cells, cells grown on 10 mm lysine-coated coverslips were incubated with the AuNP–Apt^{His}–protein complex for 1 h before being fixed with 4% paraformaldehyde (Sigma, USA). The fluorescence emitted by the Alexa 488 (495 nm excitation, 519 nm emission)-labeled secondary antibody was detected by laser scanning confocal microscopy (Carl Zeiss ZEN 2011, Germany). The relative fluorescence intensities were measured using ImageJ software (NIH, USA).

Animal experiments

Animal experiments were carried out as described previously [13]. In brief, the complex of AuNP and B-cell lymphoma 2 interacting mediator of cell death (BIM) protein complex was injected intravenously into four-week-old female Sprague–Dawley rats at a dose of 1 mg/kg AuNP–Apt^{His} and 10 μg BIM.

Visualization of BIM protein uptake by AuNP–Apt conjugates in rat organs

Visualization of the BIM protein in rat organs was carried ou t as previously described [13]. In brief, effective delivery of Alexa 488-labeled BIM by AuNP–Apt^{His} conjugates into the organs was detected as a green signal in the sectioned organs by laser scanning confocal microscopy (Carl Zeiss ZEN 2011, Germany). The relative fluorescence intensities were measured using ImageJ software (NIH, USA).

Transmission electron microscopy

Transmission electron microscopy (TEM) was performed as previously described [13]. In brief, liver sections were fixed in Karnovsky's glutaraldehyde–paraformaldehyde mixture in 0.2 M cacodylate buffer (pH 7.4) for approximately 3 h at room temperature. The liver sections were washed with cacodylate buffer (pH 7.4) to remove the fixatives, dehydrated in an alcohol series, embedded in Spurr's resin, and sliced to a thickness of 70 nm. TEM images were taken with a JEOL model JEM-1010 system operated at 80 kV accelerating voltage, with magnification at 10,000× and 25,000×.

Results and discussion

Effects of intrinsic properties of proteins on their intracellular delivery by AuNP–Apt^{His}

Every protein has its unique physicochemical characteristics, such as molecular weight (MW), pI, and cellular localization, which can affect its transfection efficiency into mammalian cells. Although AuNPs conjugated with a His-tag DNA aptamer (AuNP–Apt^{His}) have been successfully used in transporting several proteins into mammalian cells in vitro and in vivo [13,19], it still remained uncertain whether the system could deliver any proteins with various physicochemical characteristics. For this reason, we wished to test the effects of the MW, pI, and intracellular localization of proteins on their intracellular delivery by AuNP–Apt^{His} conjugates. To do this, we used 11 recombinant proteins with a wide range of molecular weight (MW) and isoelectric point (pI) values, which are listed in Table 1. These proteins have a hexahistidine tag at either the N- or C-terminus, and five of them have been shown to be effectively delivered into mammalian cells by AuNP–Apt^{His}. When AuNP–Apt^{His} conjugates were loaded with proteins, in general, the anionicity of particles was decreased, whereas the size of particles was increased (Table 1). These changes did not appear to be associated with molecular weight or pI of proteins. Each protein (1 μM) was mixed with AuNP–Apt^{His} (1 nM) and the complexes were applied to HeLa cells. After 1 h incubation, the

Table 1
Physicochemical properties of recombinant proteins used in this study.

Protein	Molecular weight (kDa)	pI	Size (nm)[a]	ζ-Potential (mV)[b]	Localization	Reference
HPA3P	3.2	11.41	n. d.	n. d.	n.d.	[18]
TM-JM 1/2	14.1	6.79	638.3 ± 120.9	2.9	Cytoplasmic membrane	[19]
Lamin 406-567	18.7	7.16	791.8 ± 223.7	−11.79	Nucleus	[24]
RraAV1	19.4	4.08	491.9 ± 103.5	−18.03	n.d.	[25]
BIM	23	8.24	436.3 ± 76.6	−11.94	Mitochondria	[13]
RNase III	26.4	7.19	718.3 ± 191.0	−6.74	n.d.	[26]
BCL-xL	26.9	5.56	734.7 ± 174.3	−18.73	Mitochondria	[13]
Lamin 406-665	28.1	7.87	866.2 ± 208.0	−10.94	Nucleus	[24]
FOXL2	39.6	9.16	260.1 ± 210.5	−14.84	Nucleus	[27]
AcrA	42.9	8.22	1096.7 ± 265.6	−7.8	n.d.	[13]
Enolase	46.5	6.04	141.6 ± 48.9	−10.19	n.d.	[28]

n.d.: not determined.
[a] The size of AuNP–Apt^{His}–protein complex was measured.
[b] The ζ-potential of AuNP–Apt^{His}–protein complex was measured.

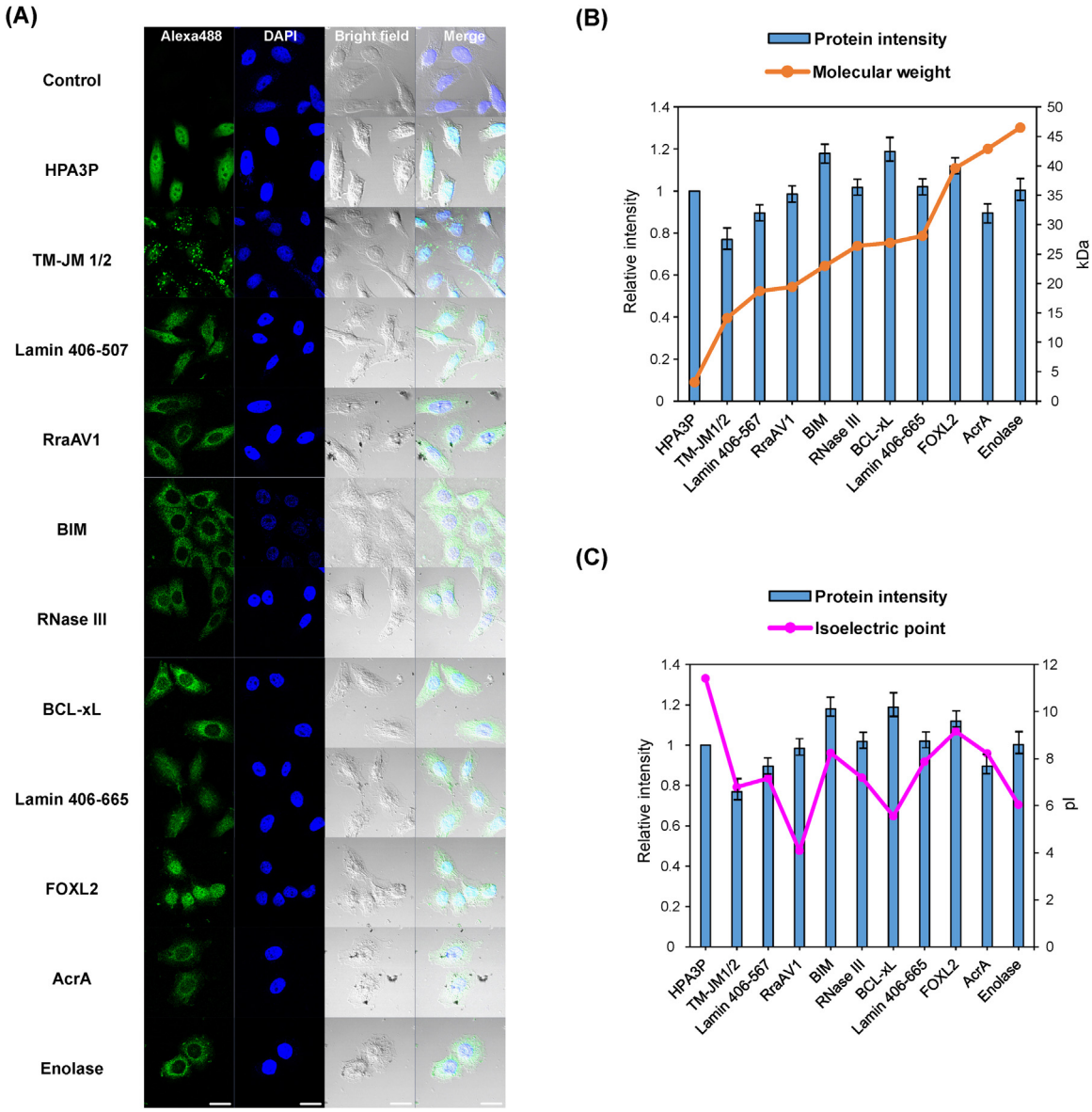

Fig. 1. Intracellular delivery of proteins by AuNP–Apt^{His}. (For interpretation of the references to color in this figure legend, the reader is referred to the web version of this article.)
(A) To assess the efficient delivery of AuNP–Apt^{His}–protein into cells, HeLa cells were immunostained with a monoclonal anti-His-tag antibody and Alexa 488-rabbit IgG. Representative confocal fluorescence microscopy images of the HeLa cells indicate the protein signal (green). Nuclei were stained with DAPI. Representative images were acquired under a 40× water-immersion objective. Scale bars = 20 μm. Alexa 488: The fluorescence channel of Alexa 488 (495 nm absorption, 519 nm emission), DAPI: the fluorescence channel of DAPI (4′, 6-diamidino-2-phenylindole, 358 nm absorption [ultraviolet], 461 nm emission), bright field: the bright-field image of HeLa cells, merge: merged channel from Alexa 488, DAPI, and bright field channels. (B and C) The relative fluorescence intensities in the HeLa cells were measured using ImageJ software. The relative amounts of other proteins delivered were compared by setting the amount of HPA3P to 1.

cells were immunostained with an Alexa 488 labeled-polyclonal antibody to His-tag and subjected to confocal microscopy analysis. The results showed no clear effects of the MW, pI, and cellular localization of the proteins on the efficiency of their intracellular delivery by AuNP–Apt^{His} (Fig. 1), implying that the system can be used for the intracellular delivery of any protein with a His-tag. We previously showed that several of these proteins (BIM, FOXL2, TM-JM1/2, and AMPs) were biologically functional in mammalian cells [13,19,20], showing the potential applications of this system in various fields of biomedicine.

Effect of cell type on intracellular protein delivery by AuNP–Apt^{His}

Our previous studies showed that AuNP–Apt^{His} conjugates are able to deliver recombinant proteins into several types of mammalian cells [13,19]. We further investigated the ability of the conjugates to deliver proteins into mammalian cells that are known to be difficult to transfect with biomaterials, including DNA, RNA, and proteins. For these experiments, we chose cervical squamous carcinoma primary cells and J1 mouse embryonic stem cells, which are known as not fast-dividing cells compared with those derived from cancers such as HeLa and 293T cells. We also

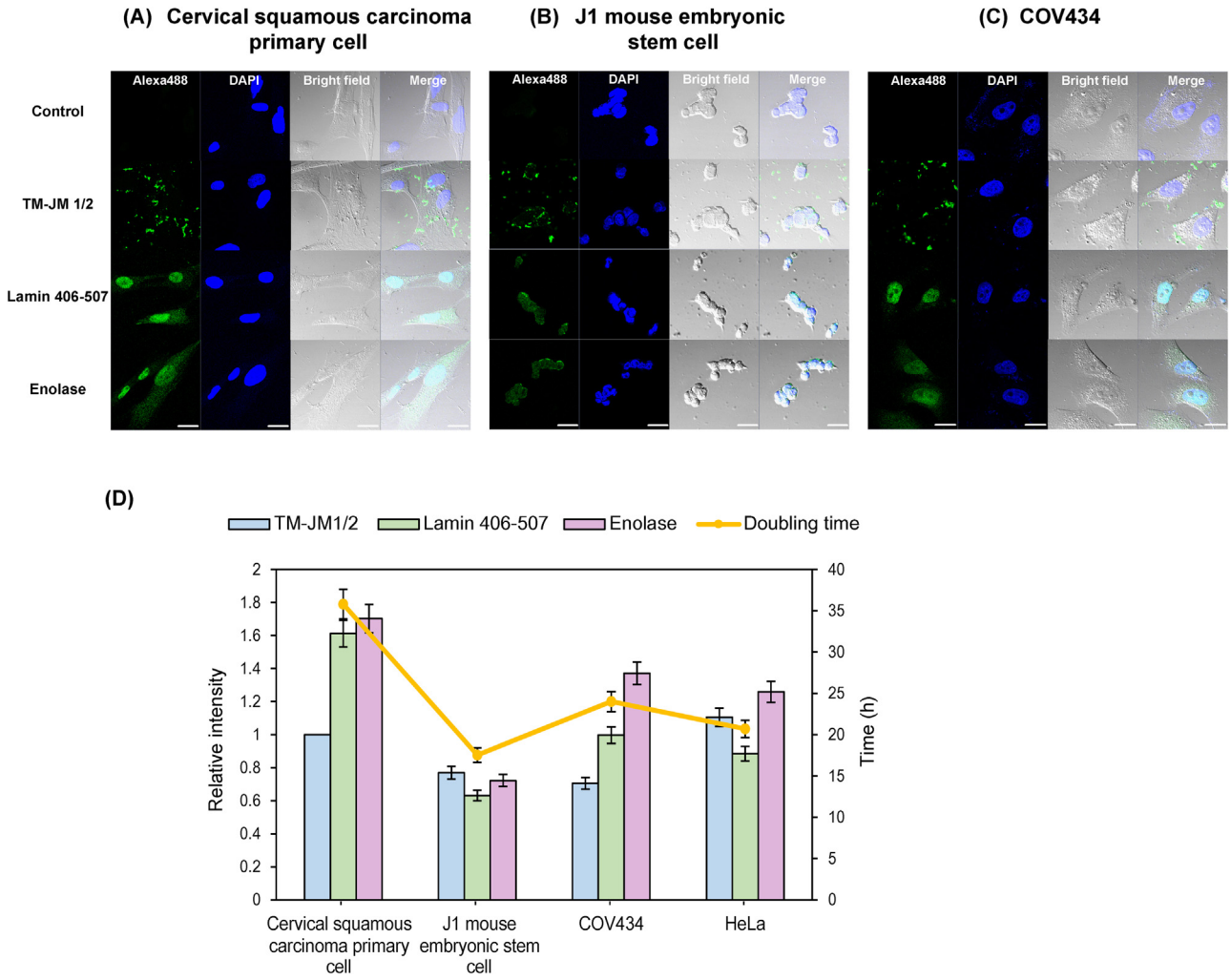

Fig. 2. Efficient delivery of the proteins into different cell types.
(A) Cervical squamous carcinoma primary cells, (B) J1 mouse embryonic stem cells, and (C) COV434 cells were incubated with AuNP–Apt^{His} (1 nM) or AuNP–Apt^{His}–protein complexes for 1 h and intracellular delivery was measured by confocal microscopy. Representative images were acquired under a 40× water-immersion objective. Scale bars = 20 μm. Alexa 488: the fluorescence channel of Alexa 488 (495 nm absorption, 519 nm emission), DAPI: the fluorescence channel of DAPI (4′, 6-diamidino-2-phenylindole, 358 nm absorption [ultraviolet], 461 nm emission), bright field: the bright-field image of cells, merge: merged channel from Alexa 488, DAPI, and bright field channels. (D) The relative fluorescence intensities in the different cell types were measured using ImageJ software. The relative amounts of TM-JM 1/2, Lamin 406-567, and Enolase delivered into different kinds of cells were compared by setting the amount of TM-JM1/2 in cervical squamous carcinoma primary cells to 1.

used COV434 cells, which are derived from a juvenile-type granulosa cell tumor [21]. Unlike other stem cells, the growth rate of J1 mouse embryonic stem cells was comparable to those of COV434 and HeLa cells whereas cervical squamous carcinoma primary cells divided much more slowly than other cells used in this experiment (Fig. 2D). The results showed that the conjugates efficiently delivered several proteins (TM-JM 1/2, Lamin 406-507, and Enolase) into these cells without showing noticeable cell-type-dependent variations (Fig. 2), indicating the versatile application of this AuNP–Apt^{His} system for delivering proteins into difficult-to-transfect cells.

Biodistribution of intravenously administrated proteins by AuNP–Apt^{His}

Once administrated, many protein drugs should be able to carry out their intended pharmacological action in the systemic circulation. We further tested whether this AuNP–Apt^{His} system could be applied to the systemic delivery of proteins into living organisms. To study the time-course biodistribution, AuNP–Apt^{His} loaded with Alexa 488-labeled BIM protein was injected into the tail vein of rats at a concentration at which no significant systemic toxicity was observed (1 mg/kg of body weight) [13]. Seven organs (brain, heart, kidney, liver, ovary, spleen, and thymus) were collected at 0, 1, 6, 12, and 24 h post protein dosing. As shown in Fig. 3A, strong green signals of Alexa 488-labeled BIM protein were observed in several tissues at different time points post injection. Signals of Alexa 488-labeled BIM proteins were very low in the brain, probably due to the brain barrier, whereas accumulation of proteins was observed in several other organs (Fig. 3A). These data correlated well with the BIM protein levels determined by confocal imaging, showing that the AuNP–Apt^{His} system can deliver proteins intravenously into rat organs with different efficiencies—higher in the heart, kidney, liver, and spleen than in the brain, ovary, and thymus (Fig. 3B).

We further analyzed the location and morphology of AuNP–Apt particles in the liver tissues, using TEM (Fig. 3C). The AuNPs were found predominantly in Kupffer cells, in aggregated form. Fewer particles were in endothelial cells and in hepatocytes, where they appeared mostly as non-aggregated particles. This clearance mechanism of the AuNP particles resembles the ones typically observed for other 10–20 nm AuNP-based nanocarriers [22,23].

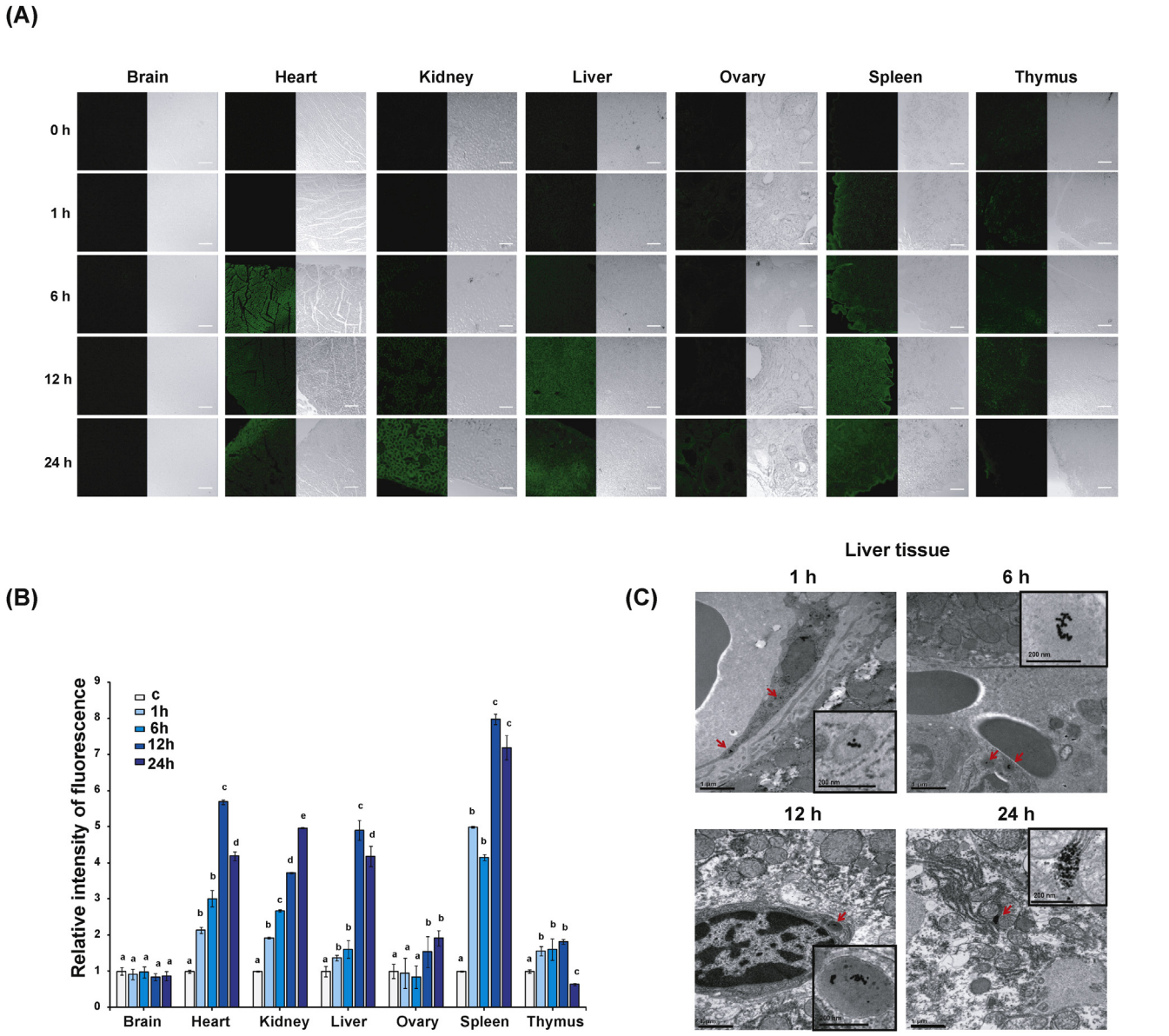

Fig. 3. Systemic delivery of BIM protein by AuNP–Apt^{His} conjugates in rats.
(A) AuNP–Apt^{His} (1 mg/kg of body weight) loaded with 10 μg Alexa 488-labled BIM protein was IV-injected once into the tail vein of rats. The rats were euthanized at 0, 1, 6, 12, and 24 h post injection, and organs were retrieved. The representative confocal fluorescence microscopy images depicted were used to detect Alexa 488-labled BIM protein in the organ sections. Scale bars = 200 μm. (B) The relative fluorescence intensities in the organ sections were measured using ImageJ software. Results (mean ± SEM) were obtained from three rats. The values are shown by setting intensities of fluorescence from organ treated with AuNP–Apt^{His} as 1. Statistically significant values are indicated with different letters ($P < 0.05$). (C) TEM of the AuNP–Apt^{His}–BIM protein complex. Sections from the liver used in (A) were processed following standard electron microscopy methods. Representative images are shown at 10,000× (left image) and 25,000× (right image) magnification.

Conclusions

Our results showed that the AuNP–Apt system can efficiently deliver recombinant proteins into mammalian cells in a manner independent of size, pI, and cellular localization of the proteins, as well as of cell types. Since the AuNP–Apt system can deliver proteins intravenously into rat organs, with proper modifications that include co-loading of cell-type specific ligands and activator molecules, it can be used for the delivery of therapeutic protein drugs into animals. Our results demonstrate that this system can serve as an innovative platform for the delivery of recombinant proteins into mammalian living systems, which we believe has open-ended applications for the development of protein-based biomedical technologies.

Acknowledgements

This work was supported by grants (NRF-2014R1A2A2A09052791; NRF-2011-0021810) from the National Research Foundation of Korea. It was also supported by the Strategic Initiative for Microbiomes in Agriculture and Food (914010-04-3-HD020), Ministry of Agriculture, Food, and Rural Affairs, Republic of Korea.

References

[1] V. Torchilin, Drug Discov. Today Technol. 5 (2008) e95.
[2] M. Yu, J. Wu, J. Shi, O.C. Farokhzad, J. Control. Release 240 (2016) 24.
[3] Z. Gu, A. Biswas, M. Zhao, Y. Tang, Chem. Soc. Rev. 40 (2011) 3638.

[4] I. Green, R. Christison, C.J. Voyce, K.R. Bundell, M.A. Lindsay, Trends Pharmacol. Sci. 24 (2003) 213.
[5] L.R. Brown, Expert Opin. Drug Deliv. 2 (2005) 29.
[6] L.N. Patel, J.L. Zaro, W.C. Shen, Pharm. Res. 24 (2007) 1977.
[7] B.S. Weeks, D.M. Lieberman, B. Johnson, E. Roque, M. Green, P. Loewenstein, E. H. Oldfield, H.K. Kleinman, J. Neurosci. Res. 42 (1995) 34.
[8] F. Zeng, H. Lee, C. Allen, Bioconjug. Chem. 17 (2006) 399.
[9] M.E. Gindy, S. Ji, T.R. Hoye, A.Z. Panagiotopoulos, R.K. Prud'homme, Biomacromolecules 9 (2008) 2705.
[10] E. Jule, Y. Nagasaki, K. Kataoka, Bioconjug. Chem. 14 (2003) 177.
[11] S.L. Hussey, B.R. Peterson, J. Am. Chem. Soc. 124 (2002) 6265.
[12] A.B. Hill, M. Chen, C.K. Chen, B.A. Pfeifer, C.H. Jones, Trends Biotechnol. 34 (2016) 91.
[13] S.M. Ryou, J.H. Yeom, H.J. Kang, M. Won, J.S. Kim, B. Lee, M.J. Seong, N.C. Ha, J. Bae, K. Lee, J. Control. Release 196 (2014) 287.
[14] M. McKeague, M.C. Derosa, J. Nucleic Acids 2012 (2012) 748913.
[15] N.L. Rosi, D.A. Giljohann, C.S. Thaxton, A.K. Lytton-Jean, M.S. Han, C.A. Mirkin, Science 312 (2006) 1027.
[16] J.H. Kim, H.H. Jang, S.M. Ryou, S. Kim, J. Bae, K. Lee, M.S. Han, Chem. Commun. (Camb.) 46 (2010) 4151.
[17] D. Kim, Y.Y. Jeong, S. Jon, ACS Nano 4 (2010) 3689.
[18] J.K. Lee, S.C. Park, K.S. Hahm, Y. Park, Biomaterials 35 (2014) 1025.
[19] D. Kim, J.H. Yeom, B. Lee, K. Lee, J. Bae, S. Rhee, Biochem. Biophys. Res. Commun. 464 (2015) 392.
[20] J.H. Yeom, B. Lee, D. Kim, J.K. Lee, S. Kim, J. Bae, Y. Park, K. Lee, Biomaterials 104 (2016) 43.
[21] S. Jamieson, R. Butzow, N. Andersson, M. Alexiadis, L. Unkila-Kallio, M. Heikinheimo, P.J. Fuller, M. Anttonen, Mod. Pathol. 23 (2010) 1477.
[22] W.S. Cho, M. Cho, J. Jeong, M. Choi, H.Y. Cho, B.S. Han, S.H. Kim, H.O. Kim, Y.T. Lim, B.H. Chung, J. Jeong, Toxicol. Appl. Pharmacol. 236 (2009) 16.
[23] M. Wojnicki, M. Luty-Blocho, M. Bednarski, M. Dudek, J. Knutelska, J. Sapa, M. Zygmunt, G. Nowak, K. Fitzner, Pharmacol. Rep. 65 (2013) 1033.
[24] Y.S. Jung, S.J. Lee, S.H. Lee, J.Y. Chung, Y.J. Jung, S.H. Hwang, N.C. Ha, B.J. Park, Cell Cycle 12 (2013) 2277.
[25] M. Lee, J.H. Yeom, S.H. Sim, S. Ahn, K. Lee, Curr. Microbiol. 58 (2009) 349.
[26] S.H. Sim, J.H. Yeom, C. Shin, W.S. Song, E. Shin, H.M. Kim, C.J. Cha, S.H. Han, N.C. Ha, S.W. Kim, Y. Hahn, J. Bae, K. Lee, Mol. Microbiol. 75 (2010) 413.
[27] M. Park, E. Shin, M. Won, J.H. Kim, H. Go, H.L. Kim, J.J. Ko, K. Lee, J. Bae, Mol. Endocrinol. 24 (2010) 1024.
[28] G.G. Liou, H.Y. Chang, C.S. Lin, S. Lin-Chao, J. Biol. Chem. 277 (2002) 41157.